Title

Analysis of the Reaction Mechanism and Catalytic Activity of Metal-Substituted Beta Zeolite for the Isomerization of Glucose to Fructose

Journal

ACS Catalysis, 4(5)

ISSN

2155-5435

Authors

Li, Yi-Pei
Head-Gordon, Martin
Bell, Alexis T

Publication Date

2014-05-02

DOI

10.1021/cs401054f

Peer reviewed

ACS Catalysis

Research Article

pubs.acs.org/acscatalysis

Analysis of the Reaction Mechanism and Catalytic Activity of Metal-Substituted Beta Zeolite for the Isomerization of Glucose to Fructose

Yi-Pei Li,[†] Martin Head-Gordon,[‡] and Alexis T. Bell*[,†]

[†]Department of Chemical and Biomolecular Engineering, University of California, Berkeley, California 94720-1462

[‡]Department of Chemistry, University of California, Berkeley, California 94720-1462

Supporting Information

ABSTRACT: Glucose–fructose isomerization mediated by Sn-BEA is investigated using an extended QM/MM model containing 208 tetrahedral atoms. The isomerization mechanism consists of a sequence of ring-opening, isomerization, and ring-closing processes, consistent with the previously reported experimental observations. In agreement with the experimentally observed kinetic isotope effect, the rate-determining step is found to involve a hydride shift from the C_2 carbon to the C_1 carbon. The apparent activation energy for the rate-limiting step is 22.3 kcal/mol at 343 K. The difference in the reaction barriers for the partially hydrolyzed and the fully coordinated Sn sites was investigated using energy decomposition analysis. It is found that the higher activity of the partially hydrolyzed site comes from the extra flexibility provided by the defect in the lattice. The effect of substituting Sn in the active site by Ti, Zr, V, Nb, Si, and Ge was examined, and it was found that Sn and Zr are metals that result in the lowest reaction barrier for glucose isomerization. By using energy decomposition analysis, two physical properties are shown to contribute to the magnitude of the reaction barrier: the polarizability of the metal atom in the active site and the Brønsted basicity of the oxygen atom bound to the metal atom.

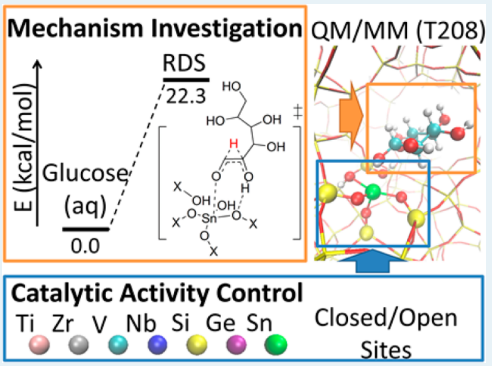

KEYWORDS: *quantum mechanics-molecular mechanics, zeolite, catalysis, glucose isomerization, reaction mechanism, energy decomposition analysis*

INTRODUCTION

Hydroxymethylfurfural (HMF) is a promising building block platform that can be converted to a wide variety of products.[1,2] For example, 2,5-dimethylfuran (DMF), a potential biofuel, can be produced by hydrogenolysis of HMF over a Cu-Ru/C catalyst.[1] HMF can also be upgraded to larger organic molecules by aldol condensation with ketones over a basic catalyst (NaOH).[3] The subsequent hydrogenation/dehydration of the condensation products over bifunctional catalysts with metal and acid sites produces diesel fuel range linear alkanes.[4] It is well-known that HMF can be obtained by dehydration of fructose, although developing an industrially viable process to prepare HMF is challenging. Previous studies showed that mediated by liquid or solid acid catalysts, fructose can be dehydrated in aqueous solutions, although the selectivity toward HMF is not satisfactory due to the formation of levulinic acid, formic acid, and humins.[5,6] Much higher yields to HMF were obtained by conversion of carbohydrates in ionic liquids.[7] It was shown that in ionic liquids, not only fructose[8−13] but also glucose,[8,9,13−16] which is a much cheaper carbohydrate, can be converted to HMF with good yields. However, it is considered costly to use ionic liquids and the product recovery and recycling operations are expected to be complex issues.[17] The potentially environmental impact also makes the conversion of carbohydrate to HMF in ionic liquids not a preferential option for mass production.

A recent study has shown that a Beta zeolite containing framework Sn atoms (Sn-BEA) will catalyze the isomerization of glucose to fructose with high activity and selectivity in aqueous solutions over a wide range of temperatures.[18] The fructose produced this way can then be converted readily to HMF by acid-catalyzed dehydration.[19] Studies of the mechanism of glucose to fructose isomerization over Sn-BEA suggest that the reaction occurs via three steps, as shown in Scheme 1.[20] On the basis of the NMR and IR observations of the acyclic form of fructose, it is proposed that the reaction is initiated by opening of the six-membered ring of glucopyranose to form acyclic glucose, which then undergoes isomerization to the acyclic form of fructose and subsequent ring closure to form the furanose product.[20] Evidence from ^{1}H and ^{13}C NMR studies conducted on glucose deuterated at the C_2 position indicate that the isomerization of acyclic glucose to fructose proceeds by way of an intramolecular hydride shift. The observation of a significant H/D kinetic isotope effect suggests that the hydride shift is the rate-limiting step.[21]

The structure of the active site responsible for the glucose–fructose isomerization in Sn-BEA has been investigated, because it has been shown that there are two types of active

Received: November 12, 2013
Revised: March 12, 2014
Published: April 4, 2014

Scheme 1. Schematic Representations of the Isomerization of Glucopyranose to Fructofuranose[a]

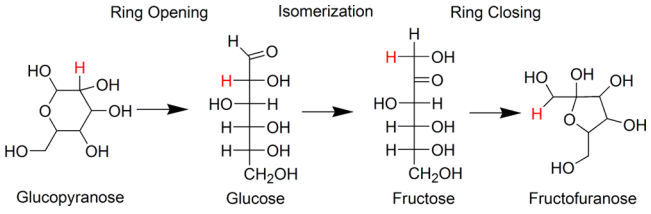

[a]The hydrogen atom marked as red is the one that performs hydride shift.

sites in Sn-BEA: one is the partially hydrolyzed Sn site (open site), the other is the fully coordinated site (closed site), as illustrated in Scheme 2.[22] The open sites have been shown to

Scheme 2. Structures of Fully Coordinated (Closed) and Partially Hydrolyzed (Open) Sn Sites[a]

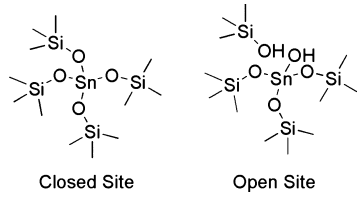

[a]Three-dimensional structures can be found in Figure S1 in Supporting Information.

be more active than the closed sites for the Baeyer–Villiger and Meerwein–Ponndorf–Verley reactions.[22,23] The role of closed and open sites for glucose to fructose isomerization has been examined theoretically by Bermejo-Deval et al.[20] This work was performed using a small (T4) cluster representation of the active site, which was assumed to be fully solvated by water. The highest reaction barrier for the closed sites was found to be ∼8 kcal/mol higher than that for the open sites, suggesting the open sites are responsible for the glucose–fructose isomerization. The reaction barrier over Ti open sites was also calculated in the same work and was shown to be ∼10 kcal/mol higher than that of the Sn open sites,[20] consistent with the experimental observation that Sn-BEA is more active than Ti-BEA.[18] Although it has provided useful insights, the very minimal model of the active site used in this work could not explain why the hydrophobic environment of the zeolite is necessary for the isomerization process,[24] the reason for the higher activity of the open site, and the role of the zeolite pore walls in stabilizing intermediates and transition-state species produced along the reaction pathway.[25] Yang et al. have attempted to address these questions using periodic boundary density functional theory (DFT) calculations,[26] and they have suggested that the activity of the open site is similar to that of the closed site and the presence of an extended silanol nest in the vicinity of the site due to vacancy defects is necessary to promote the reaction. This finding does not support the conclusion drawn by Bermejo-Deval et al. that the open site is more active. However, Rai et al. recently proposed a mechanism in which the silanol group of the open site directly participates in the rate-limiting transition state, implying that the activities of open and closed sites are different.[27] The discrepancy of the conclusions drawn by different authors leaves the role of closed and open sites for glucose to fructose isomerization as an open question requiring further investigation.

In the present study, we have analyzed the energetics of glucose-to-fructose isomerization catalyzed by Sn-BEA over open and closed sites by means of quantum mechanics/molecular mechanics (QM/MM) using a large cluster representation of the active site and the surrounding zeolite involving 208 tetrahedral atoms (T208) to capture the confinement and dispersion effects of the pores. These efforts have led to a reaction mechanism that is consistent with the deductions drawn from experimental observations and to an activation barrier for glucose to fructose isomerization on an open Sn site that is in very good agreement to that observed experimentally. We have also carried out a systematic study of the catalytic activities of zeolites containing Ti, Zr, V, Nb, Si, or Ge at the active site instead of Sn. Using energy decomposition analysis (EDA),[28] two descriptors of site activity were identified. Owing to the fact that the oxygen atom binding to

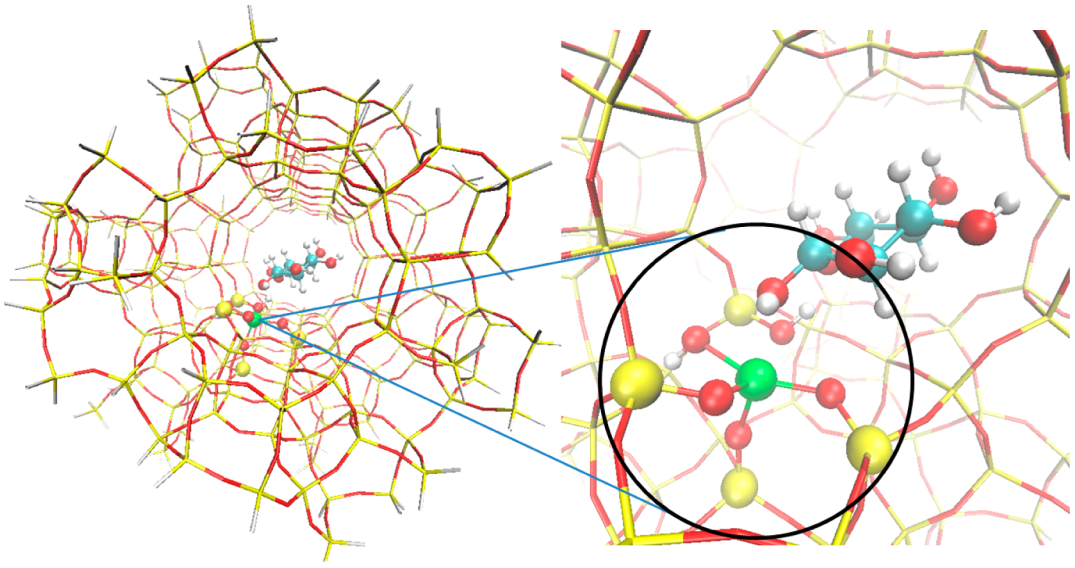

Figure 1. Sn-BEA QM/MM model (T208), where the partially hydrolyzed T2 site is shown. Spherical atoms are QM atoms, others are MM atoms.

dx.doi.org/10.1021/cs401054f | ACS Catal. 2014, 4, 1537–1545

the heteroatom in an active site acts like a Brønsted base in the rate-limiting step, the first descriptor is the negative partial charge on the oxygen atom, which correlates closely with the magnitude of the electrostatic stabilization between a site and a substrate. The second descriptor is the radius of the heteroatom, which correlates with the polarizability of the active center, determining the energy penalty associated with distortion of the geometry of the active site from its resting geometry to the geometry in the transition state. The geometry distortion penalty of the active site is also shown to be affected by the structure of the site, which explains why a partially hydrolyzed open site is more active than a fully coordinated closed site.

THEORETICAL METHODS

Zeolite Model Geometries. The structure of BEA was described by a T208 cluster with the position of all Si and O atoms determined by the crystallographic structure of BEA.[29] The cluster was terminated with hydrogen atoms by replacing the terminal oxygen atoms. Sn-BEA was produced by replacing a Si atom in the framework by a Sn atom. Though the BEA framework has nine unique T-atom positions, there is evidence that two sites are favored for Sn atom substitution,[30,31] the T1 and T2 sites in the nomenclature of Newsam et al.[29] For this study, we considered the Sn atom to be in the T2 site, as shown in Figure 1.

QM/MM Computations. Implementation of the QM/MM model in this work followed the scheme described previously.[32] As shown in Figure 1, glucose and a T5 cluster encompassing the active center were described by QM, whereas the rest of the zeolite was described by MM using a standard force field of the CHARMM type.[33−35] All geometry optimizations were performed with relaxation of the atoms only in the QM region, while maintaining all of the MM atoms frozen. Because the MM atoms are held fixed, the only relevant terms in the force field are the interactions between atoms in the MM part of the cluster with the atoms in the QM region. The electrostatic part of this interaction, is described by

$$V_{\mathrm{QM/MM}} = \sum_{ij} \frac{q_j}{4\pi\varepsilon_0 r_{ij}} \tag{1}$$

where $V_{\mathrm{QM/MM}}$ is the electric potential in the QM Hamiltonian due to all the MM atoms; r_{ij} is the distance between particles i and j, where particle i is in the QM region and particle j is in the MM region; q_j is the charges on particles j, which is a force field parameter; and ε_0 is the permittivity of free space. The Lennar−Jones interaction E_{LJ} is given by

$$E_{\mathrm{LJ}} = \sum_{ij} \varepsilon_{ij}\left[\left(\frac{R_{ij}}{r_{ij}}\right)^{12} - 2\left(\frac{R_{ij}}{r_{ij}}\right)^{6}\right] \tag{2}$$

where $\varepsilon_{ij} = (\varepsilon_i\varepsilon_j)^{1/2}$ and $R_{ij} = (R_i + R_j)/2$, R_i is the van der Waals radius, and ε_i is the characteristic energy for the Lennard−Jones potential. These expressions require three parameters for each atom type. The parameters for atoms of the zeolite cluster are listed in Table 1. These values have been recently reoptimized to yield improved accuracy for adsorption energies of organic molecules in zeolites.[36] Standard CHARMM parameters were used for the atoms of the substrates.[37]

Geometry optimizations and single-point energy calculations were performed using density functional theory (DFT) at the

Table 1. Charge and Lennard−Jones Parameters for O and Si Used in the QM/MM Portion of This Work

Q_{Si}	Q_O	ε_{Si} (kcal/mol)	R_{Si} (Å)	ε_O (kcal/mol)	R_O (Å)
0.7	−0.35	0.047	2.2	0.018	1.77

ωB97X-D[38,39]/Def2-SV(P) and ωB97X-D/Def2-TZVPD levels of theory, respectively. All calculations were carried out using a development version of the Q-Chem software package.[40] Partial charges on atoms were calculated using natural bond orbital (NBO) analysis.[41] Reaction intermediates were guessed by hand followed by standard geometry optimizations to refine the structures. The transition structures connecting intermediates were found by the freezing string method[42] followed by local optimization. Kinetically uncompetitive pathways were discarded leading to a final viable reaction mechanism. The reported numbers are ground-state electronic energies without zero point vibrational and thermal corrections unless otherwise noted.

Solvation of Sugars. Though the isomerization of glucose to fructose occurs in aqueous solution, the solvation effect is believed to be negligible in the zeolite system, because it has been shown that the molecular sieves have to be highly hydrophobic to maintain good activity for the reaction.[43] Therefore, no explicit water molecule or solvation model is used to treat the substrate−catalyst complex. However, to have a reasonable comparison with the experimentally measured reaction barrier, the energies of the isolated catalyst and the solvated glucopyranose, instead of glucopyranose in gas phase, were chosen as the references for the potential energy surface

$$\begin{aligned} E &= E(\mathrm{S{\cdot}C}) - E(\mathrm{C}) - E_{\mathrm{aq}}(\mathrm{S}) \\ &= E(\mathrm{S{\cdot}C}) - E(\mathrm{C}) - [E(\mathrm{S}) + \Delta E_{\mathrm{solvation}}(\mathrm{S})] \end{aligned} \tag{3}$$

where $E(\mathrm{S{\cdot}C})$ is the energy of the substrate-catalyst complex, $E(\mathrm{C})$ is the energy of the catalyst, $E_{\mathrm{aq}}(\mathrm{S})$ is the energy of the solvated glucopyranose, $E(\mathrm{S})$ is the energy of glucopyranose in gas phase, and $\Delta E_{\mathrm{solvation}}(\mathrm{S})$ is the solvation energy of glucopyranose in water. Because $\Delta E_{\mathrm{solvation}}(\mathrm{S})$ is a constant along the reaction pathway and plays no role in determining the reaction mechanism, it was estimated using the SM8 solvation model[44] at the ωB97X-D/6−31+G** level of theory.

RESULTS AND DISCUSSION

Reaction Mechanism. Because the open sites have been shown to be more active than the closed sites for Baeyer−Villiger reaction and Meerwein−Ponndorf−Verley reaction,[22,23] and were believed to be responsible for the isomerization of glucose to fructose,[20] the open site is chosen to study the reaction energetics in this work. The difference in the reaction barriers for the open and closed sites is discussed below.

The best calculated mechanism of glucose−fructose isomerization mediated by Sn-BEA and the associated potential energy surface are shown in Figure 2. The mechanism consists of a sequence of ring-opening (species 1 to 5), isomerization (species 6 to 10), and ring-closing (species 11 to 13) processes, which are consistent with the mechanism shown in Scheme 1. Because a significant kinetic isotope effect has been observed experimentally for the hydride-transfer step,[21] the transitions from states 5 to 6 and from 10 to 11, which do not alter any chemical bonds, cannot be rate-limiting and, therefore, are not calculated.

dx.doi.org/10.1021/cs401054f | ACS Catal. 2014, 4, 1537−1545

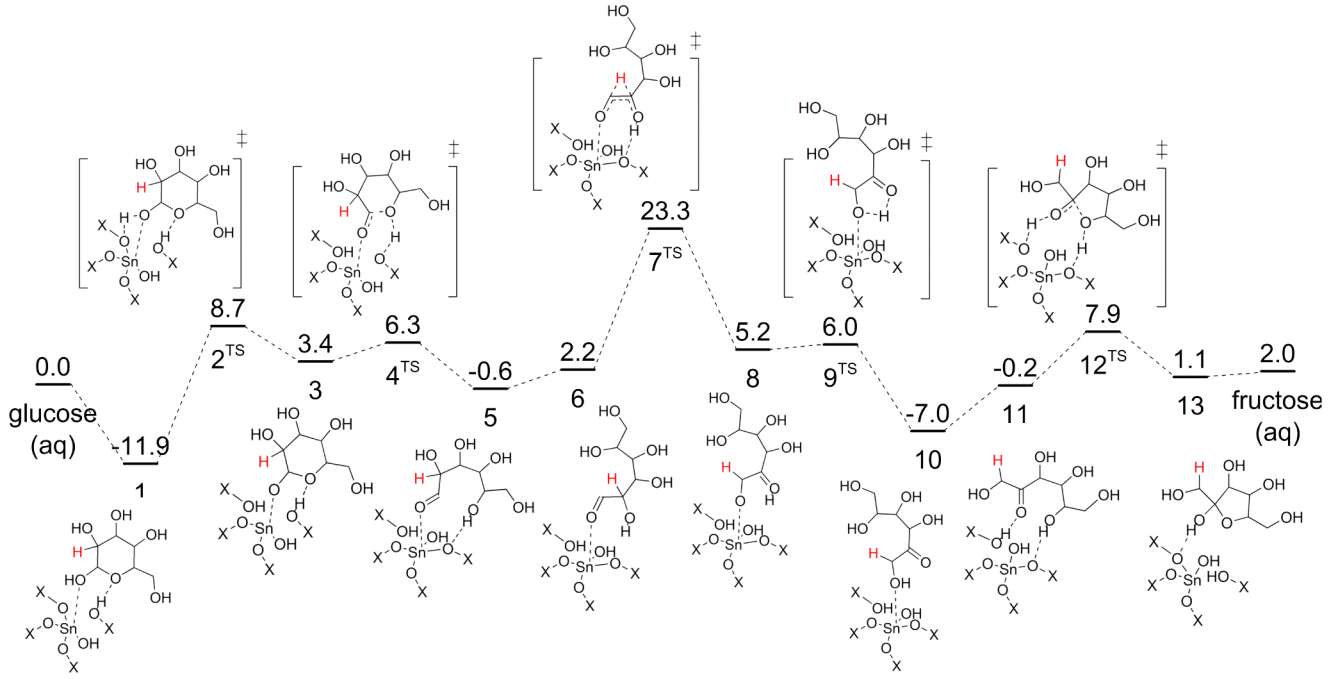

Figure 2. Potential energy surface of glucose–fructose isomerization mediated by the T2 Sn-BEA open site. All energies are reported in kcal/mol and are with respect to glucopyranose in aqueous solution and Sn-BEA model. The hydrogen atom marked as red is the one that performs hydride shift. Three-dimensional structures of these species can be found in Figure S2 in Supporting Information.

The first step of the mechanism is the binding of glucopyranose to the active site by coordinating the oxygen atom of the hydroxyl group on the C_1 carbon to the Sn center. This process is thermodynamically downhill by 11.9 kcal/mol. The interaction of the hydroxyl group of the glucopyranose with the Sn center, which acts as a Lewis acid, makes the proton of the hydroxyl group more acidic so that it can be transferred to the lattice via the transition state TS-2 with an apparent reaction barrier of only 8.7 kcal/mol. In transition state TS-4, the hydroxyl group connected to the active site acts as a Brønsted acid, donating a proton to the adsorbate resulting in the opening of the six-membered ring of the glucopyranose. The steps involved in ring opening do not require significant barriers relative to the subsequent hydride shift, which occurs via transition state TS-7. In this step, as shown in Figure 3a, the Sn atom acts as a Lewis acid that polarizes the carbonyl group of the ring-opened glucose so that the H atom (shown in red in Figure 2) can shift from the C_2 carbon to the C_1 carbon.

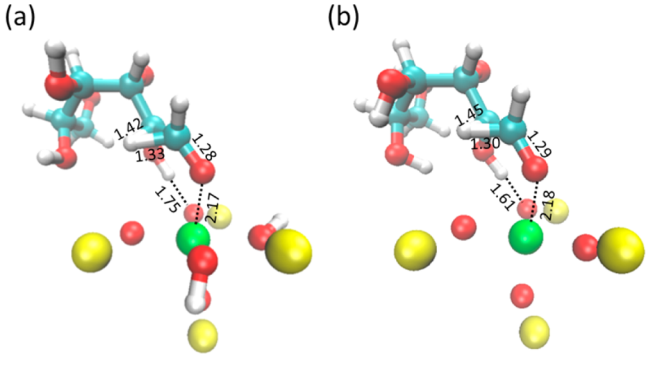

Figure 3. Three-dimensional structures of TS-7 over (a) the open and (b) the closed Sn sites. For clarity, the extended zeolite cluster is not shown. Selected bond lengths are given in Å.

Assuming that occupancy of the active sites is very low (see Text S1 in Supporting Information for a discussion of this point), the apparent reaction barrier for hydride transfer is determined to be 23.3 kcal/mol. Taking the ground-state rigid-rotor harmonic oscillator vibrational correction and thermal correction into account, the apparent activation energy is determined to be 22.3 kcal/mol at 343 K, in very good agreement with the experimentally reported value of 21.2 ± 0.7 kcal/mol (343–373 K).[20] Because the barrier for hydride transfer is the highest one along the reaction pathway, we conclude that it is the rate-limiting step. This finding supports the deduction drawn by Bermejo-Deval et al. based on the observation of a kinetic isotope effect when the C_2 carbon of glucose was labeled with duterium.[20,21] After the hydride shift, the protonated carbonyl group on the C_2 carbon transfers the proton to the alkoxide group on the C_1 carbon through the transition state TS-9, which exhibits an apparent reaction barrier of 6.0 kcal/mol. The last step is the conversion of fructose from its acyclic to its cyclic conformation to form the product fructofuranose. This process involves the transfer of two protons between the fructose molecule and the active site as shown by the transition state TS-12, which has a relatively low reaction barrier of 7.9 kcal/mol.

The mechanism shown in Figure 2 is different from those proposed previously by other authors based on computational studies,[20,26,27] but is in better agreement with experimental results known to date. These differences can be due to different computational methods (DFT functional, basis set), or more likely, different treatment of the extended environment (small vs medium clusters vs periodic or QM/MM models) and the possibility of missing stationary points. Bearing in mind these issues, we turn to a comparative discussion. Bermejo-Deval et al. proposed that after the ring opening process, the hydride transfer is activated by a proton transfer from the C_2 hydroxyl group to the basic stannanol of the Sn open site and both of the

dx.doi.org/10.1021/cs401054f | ACS Catal. 2014, 4, 1537–1545

oxygen atoms at the C_1 and C_2 positions coordinate to the Sn center while the hydride is transferred.[20] Such a bidentate mode for the hydride shift is different from the monodentate mode we propose here (TS-7). Though Bermejo-Deval et al. showed that this bidentate hydride shift is the highest energy state along the pathway using a T4 cluster representation for the active site, which agrees with experimentally observed kinetic isotopic effect, Yang et al. showed that taking extended zeolite cluster into account using periodic boundary DFT, the calculated activation energy (see Text S2 in Supporting Information for how this number is derived) for this bidentate mode is 7.8 kcal/mol higher than the value measured experimentally.[26] Better agreement with the experimentally measured barrier was achieved by assuming that an extended silanol nest due to vacancy defects was present in the vicinity of the active site. But this defect assumption is not consistent with the experimental observation that the reaction rate is greatly decreased when a highly defective molecular sieve is used.[43] To perform a direct comparison between the nondefective bidentate pathway and the monodentate one proposed here, an attempt was made to reproduce the bidentate mode using our QM/MM model; however, this attempt failed, most likely because the bidentate intermediate and transition state do not exist in our extended model. By contrast, in the previous studies, either the extended zeolite cluster was ignored[20,27] or one of the Si atoms neighboring the Sn was removed when an open site was constructed.[26] Because both the extended zeolite cluster and the structural integrity in the vicinity of the active site are preserved in our model, greater steric hindrance is expected, causing the formation of a bidentate complex to be unfavorable.

Interestingly, using a T9 cluster representation for the zeolite, Rai et al. also showed that a monodentate mode is more favorable than the bidentate mode for the hydride shift.[27] They suggested that only the oxygen atom at the C_2 position coordinates to the Sn center while the hydride is transferred and the hydride shift itself is accompanied by two concerted proton transfers, including a proton transfer from the silanol of the active site to the oxygen atom at the C_1 position. This mechanism assumes that the silanol of the active site participates in the rate-determining step and provides a good explanation for the activity difference between open and closed sites. However, it is very hard to explain the experimental observation that exchanging the adjacent hydroxyl groups of the active centers with Na^+ does not significantly alter the reaction rate.[20] Rai et al. tried to rationalize this experimental observation by postulating that water molecules could show behavior similar to the silanol group, and they will step in if no silanol is available.[27] However, we believe that the invariance of the reaction rate suggests that the rate-limiting transition state should not be affected as adjacent hydroxyl groups of the active centers are exchanged with Na^+, indicating that the hydroxyl groups of Sn or Si do not play a role in the rate-limiting step, which is consistent with the transition state we proposed for the hydride shift (TS-7). In the mechanism shown in Figure 2, the hydroxyl group of the open site is only involved in the ring opening and closing processes, which are kinetically irrelevant. Therefore, although the ring-opening and -closing processes over the open sites of the sodium form may follow pathways different from those shown in Figure 2, as long as these processes do not have barriers higher than that for TS-7 (23.3 kcal/mol), no difference in the reaction kinetics would be observed.

Comparison of Sn/Ti/Zr/V/Nb/Si/Ge Activities. To understand how the substitution of the heteroatom (M) affects catalyst performance, the apparent reaction barriers of the rate-limiting step, TS-7, were calculated by substituting Sn with Ti, Zr, V, Nb, Si, and Ge. The structure of the active sites containing tetravalent elements (Ti, Zr, Si, and Ge) is the same as that for the Sn open site, whereas for sites containing pentavalent atoms (V, Nb), ≡Sn-OH is replaced by ≡M=O (Scheme S1).[45] The computed reaction barriers are shown in Table 2. The highest barrier is for the V site, 39.0 kcal/mol. By

Table 2. Apparent Reaction Barriers of Active Sites Doped with Different Heteroatoms

	Ti	Zr	V	Nb	Si	Ge	Sn
E_a (kcal/mol)	32.1	23.5	39.0	25.7	37.4	32.2	23.3

contrast, the lowest barriers are for Sn and Zr sites, which are both about 23 kcal/mol. The reaction barrier over the Ti site is 8.8 kcal/mol higher than that of the Sn site, consistent with the experimental observation that Sn-BEA is more active than Ti-BEA.[18] Interestingly, even though the central atom acts like a Lewis acid in TS-7, there is no direct correlation between the barriers and the common descriptors of the Lewis acidity (Figure S3).

Hoping to obtain a detailed understanding of the variations in the E_a with metal composition, we carried out an energy decomposition analysis (EDA).[28] This process begins by representing the energy of the substrate−catalyst complex as the sum of energies of the substrate and catalyst and the substrate−catalyst interaction energy $\Delta E_{interaction}$. The last term can then be decomposed into physically relevant components as shown in eq 4

$$\begin{aligned} E(\mathrm{S{\cdot}C}) &= E(\mathrm{S}) + E(\mathrm{C}) + \Delta E_{interaction}(\mathrm{S{\cdot}C}) \\ &= E(\mathrm{S}) + E(\mathrm{C}) + E_{GD}(\mathrm{S}) + E_{GD}(\mathrm{C}) + E_{FRZ} + E_{POL} + E_{CT} \\ &= E(\mathrm{S}) + E(\mathrm{C}) + E_{GD}(\mathrm{S}) + E_{GD}(\mathrm{C}) + E_e + E_{CT} \end{aligned} \quad (4)$$

where E_{GD} is the energy penalty associated with geometric distortion of the isolated host and guest from their optimized geometry to the geometry that they have in the complex; E_{FRZ} is the electrostatic interaction without any relaxation of the MOs; E_{POL} and E_{CT} are the energy lowering due to the relaxation of the frozen MOs and dative charge transfer effects, respectively; and E_e is the total electrostatic interaction, which is the summation of E_{FRZ} and E_{POL}. The apparent reaction barrier can now be decomposed by substituting eq 4 into eq 3

$$\begin{aligned} E_a &= E(\mathrm{S{\cdot}C})^{\ddagger} - E(\mathrm{C}) - E_{aq}(\mathrm{S}) \\ &= E_{GD}(\mathrm{S})^{\ddagger} + E_{GD}(\mathrm{C})^{\ddagger} + E_e{}^{\ddagger} + E_{CT}{}^{\ddagger} - \Delta E_{solvation}(\mathrm{S}) \end{aligned} \quad (5)$$

where the superscript ‡ designates the energy components associated with transition structure for the rate-limiting step. To simplify the notation, the superscript ‡ will be ignored from this point.

The components comprising the reaction barriers for the rate-limiting step are depicted in Figure 4. The magnitude of $\Delta E_{solvation}(\mathrm{S})$ is not shown, because it is a constant and does not contribute to variations in E_a. The value of $E_{GD}(\mathrm{C})$ varies as the identity of the central atom is changed, suggesting that the sites with different heteroatoms have different energy penalties associated with deviations from their optimized geometries to the geometries that they have in TS-7. By contrast, because the

dx.doi.org/10.1021/cs401054f | ACS Catal. 2014, 4, 1537−1545

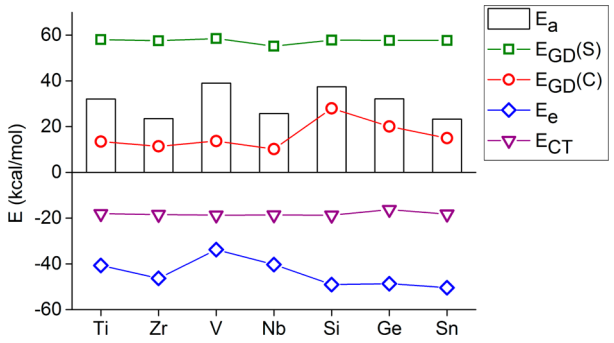

Figure 4. Energy decomposition analysis for active sites doped with different heteroatoms. The connecting lines are drawn to guide the eye.

geometry of the substrate in TS-7 is controlled not only by the active site metal but also by the extended zeolite environment, the value of $E_{GD}(S)$ is almost invariant for different active sites. The value E_e varies with the identity of M, so that it also contributes to the variation of the reaction barrier. Interestingly, the values of E_{CT} are similar for each metal. This suggests that all of the metal atoms considered have similar abilities to accept electrons from the substrate so that the charge transfer effect is not one of the main effects governing the variation in E_a.

We believe the difference in the polarizability of M contributes to the variation of $E_{GD}(C)$ with the identity of M, as evidenced by the observation that the more polarizable M is, the lower the energy penalty for distorting the geometry of the active site (Figure S4). Because the polarizability of M is proportional to the volume of the atom,[46] there is a close correlation between $E_{GD}(C)$ and R, the covalent radius of M, as shown in Figure 5. On the other hand, E_e is governed by the

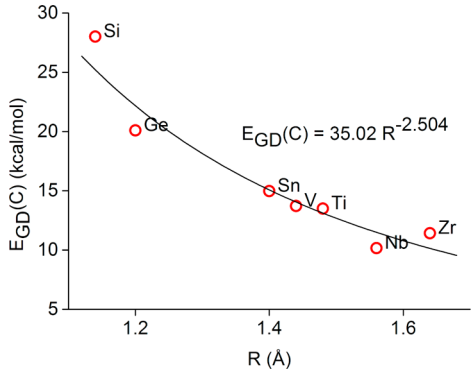

Figure 5. Correlation between geometric distortion energies of the catalyst active site, C, and the radii[47] of the heteroatoms contained in the active sites (R^2 = 0.93).

charge distribution on the active site (Figure S5), particularly Q_O, the negative charge located on the oxygen atom that the C_2 hydroxyl group points to in TS-7 (Scheme S2), as shown in Figure 6. Because Q_O can be considered as a descriptor of the Brønsted basicity of the oxygen atom, this finding suggests that the oxygen atom of the active site which acts as a Brønsted base in TS-7 plays an important role in determining E_a. The rationale for lumping E_{FRZ} and E_{POL} together as E_e in the analysis can be found in the Supporting Information (Text S3).

To correlate the reaction barriers with fundamental physical properties, the two correlations between $E_{GD}(C)$ and R, E_e and Q_O were substituted into eq 5

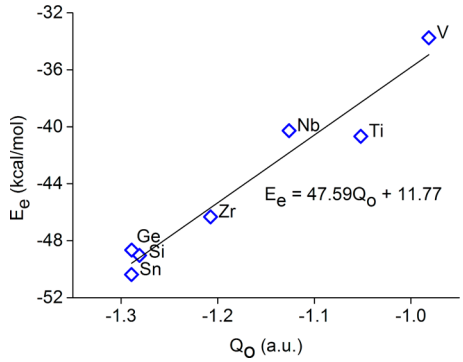

Figure 6. Correlation between the total electrostatic interactions E_e and the negative partial charge Q_O, associated with the active site O atom that will act as a Brønsted base toward a substrate C_2 hydroxyl group (R^2 = 0.95).

$$E_a = 35.02R^{-2.504} + 47.59Q_O + 11.77 + E_{GD}(S) + E_{CT} - \Delta E_{solvation}(S) \quad (6)$$

Because $E_{GD}(S)$ and E_{CT} are almost invariant with the identity of M, average values of $E_{GD}(S)$ and E_{CT} and the value of the solvation energy were substituted into eq 6 to obtain

$$E_a = 35.02R^{-2.504} + 47.59Q_O + 70.40 \quad (7)$$

Although eq 7 correlates the reaction barriers of different active sites with only two descriptors, R and Q_O, the qualitative trend in the reaction barriers with M can be captured as shown in Figure 7. To visualize the individual effects of polarizability and

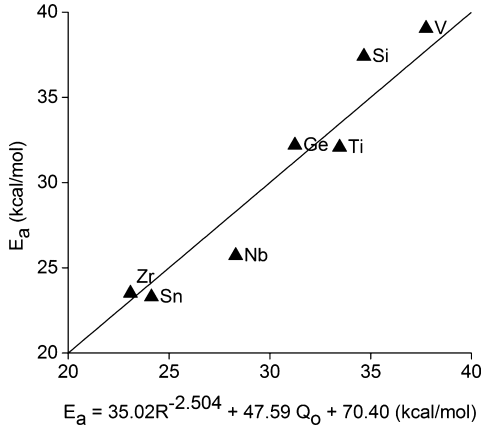

Figure 7. Parity plot for E_a calculated with QM/MM and E_a predicted by eq 7 (R^2 = 0.72).

Brønsted basicity on the reaction barriers, a contour plot of eq 7 is shown in Figure 8. The large negative charge on the O atoms connected to Sn (see Scheme S2) suggests that Sn makes these oxygen atoms become stronger Brønsted bases that can stabilize the transition state (TS-7) through electrostatic interactions. By contrast, the value of Q_O associated with the V site is low; the oxygen atoms for this site are weak Brønsted bases and, hence, provide only limited electrostatic stabilization, as shown in Figure 4, resulting in a high value of E_a. On the other hand, the large radius of Zr suggests that the Zr center is highly polarizable so that there is a low energy penalty associated with geometric distortion of the Zr site from its optimized geometry to the geometry in the transition state TS-7. Therefore, the activity of the Zr site is comparable to that

dx.doi.org/10.1021/cs401054f | ACS Catal. 2014, 4, 1537−1545

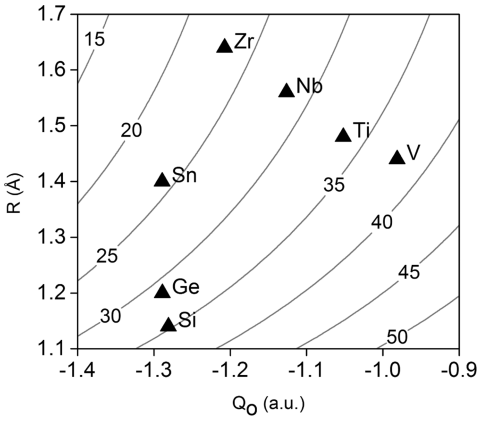

Figure 8. Correlation between apparent reaction barriers and two descriptors, radii of M and negative partial charge Q_O.

of the Sn site, although the individual contributing factors are different. Conversely, the Si site has the least polarizable center so that even though its oxygen atoms have similar Brønsted basicity to those in the Sn site, the high energy penalty of geometric distortion of the active site still leads to a high reaction barrier and makes it catalytically inactive.

For elements in the same group (e.g., Si, Ge, and Sn), the trend observed in Figure 8 is for the one with the higher atomic number has the lower reaction barrier. However, it is not always true that BEA zeolite containing heavier elements will be more active. Two interesting cases are the elements Hf and Pb, in the same groups as Zr and Sn, respectively, but in the next period. Due to lanthanide contraction, the atomic radii of Hf (1.64 Å) and Pb (1.45 Å) are not significantly increased from Zr (1.64 Å) and Sn (1.40 Å),[47] implying that the activity difference between these two pairs of elements will be mainly determined by Q_O, the descriptor of Brønsted basicity of the oxygen atoms. We found that the negative partial charge, Q_O, is increased from the Zr site (−1.22 au) to the Hf site (−1.25 au) but is decreased from the Sn site (−1.30 au) to the Pb site (−1.24 au). Because a strong Brønsted base is desirable for the reaction, this analysis suggests that the Hf site should be more active than the Zr site, but the Pb site should be less active than the Sn site. Indeed, we found that the calculated reaction barrier for the Hf site is 2.0 kcal/mol lower than that of the Zr site, and the barrier for the Pb site is 4.8 kcal/mol higher than that of the Sn site, which completely agrees with the prediction of the analysis. (The data reported in this paragraph were all calculated using the ωB97X functional because the long-range dispersion correction of ωB97X-D does not support the elements heavier than Xe to date.)

The energy decomposition analysis shows that the activity of the site with a highly polarizable center can be comparable to a site with strong Brønsted base oxygen atoms, as shown by Table 2, where the reaction barriers of Zr and Sn sites are comparable. However, we note that recent work of Gounder and Davis suggests that the competitive adsorption of solvent molecules on the active site could be strong enough to affect the activity.[43] The site with a highly polarizable center is more likely to be the victim of this effect, because water molecules could coordinate more strongly to a more polarizable center. Indeed, our calculation shows that the adsorption energy of water on the Zr site is 0.6 kcal/mol stronger than at the Sn site. If more than one water molecule can adsorb on the site, as suggested by Gounder and Davis,[43] it is possible that sites with highly polarizable centers show little activity due to severe site-blocking by solvent molecules. Therefore, if the competitive adsorption of solvent is taken into account, sites with strong Brønsted base oxygen atoms could be more desirable than sites with a highly polarizable center.

To summarize, the value of E_a is determined largely by two physical properties: the polarizability of the active center M and the Brønsted basicity of the oxygen atom in the site bound to M. Substitution of a more polarizable metal atom into the active center makes the site easier to tune to the optimum geometry in the transition state. On the other hand, the high ionicity of the oxygen−metal bond makes the oxygen atoms stronger Brønsted bases, which, in turn, governs the magnitude of the electrostatic stabilization between the transition state and the active site. The polarizability and the Brønsted basicity can be described by the radius of the heteroatom and the negative partial charge on the oxygen atom, respectively, providing clear criteria for future catalyst design.

Comparison of Closed/Open Sites Activities. To compare the activities of the closed and open sites, reaction barriers were calculated for the closed and open Sn sites and then analyzed by the EDA scheme discussed above (see Figure 3b for the 3D structure of TS-7 over the closed Sn site). Because the hydroxyl group of the open site plays a role in the ring-opening and -closing processes of the mechanism shown in Figure 2, we emphasize that the following results are based on the assumption that the site that can open and close the ring of sugar molecules operates without involvement of the hydroxyl groups associated with Sn or Si.

Figure 9 shows that the reaction barrier for the closed site is 7.1 kcal/mol higher than that for the open site, consistent with

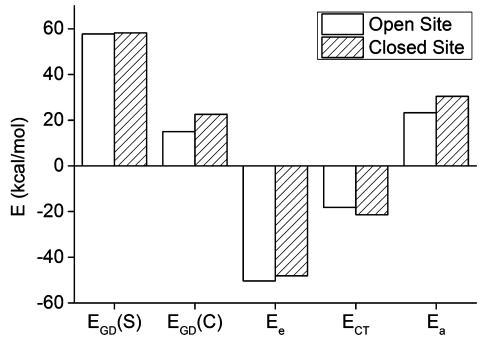

Figure 9. Energy decomposition analysis for Sn open site and closed site.

the experimental studies of the Baeyer−Villiger and Meerwein−Ponndorf−Verley reactions.[22,23] Because other components of the barriers, $E_{GD}(S)$, E_e, and E_{CT}, have a net effect that is roughly the same for the two sites, the difference in the value of E_a is mainly caused by the 7.6 kcal/mol difference in $E_{GD}(C)$, resulting from the difference in the flexibilities of the closed and open sites. The partially hydrolyzed site has a lower geometric distortion energy than the fully coordinated site because one of the Si−O−Sn bridges is "broken", thereby resulting in greater flexibility of the site. This finding demonstrates that $E_{GD}(C)$ is not controlled solely by the polarizability of M but also by the structure and connectivity of the active site.

CONCLUSIONS

A detailed mechanism of glucose−fructose isomerization mediated by Sn-BEA has been obtained using QM/MM

dx.doi.org/10.1021/cs401054f | ACS Catal. 2014, 4, 1537−1545

simulations (see Figure 2). The mechanism can be described as a sequence of ring-opening, isomerization, and ring-closing processes, which are consistent with the previously reported mechanism deduced from experimental observations. The rate-determining step does, however, differ from previous computational studies, for reasons that we have discussed in detail. The ring-opening and -closing processes do not require significant apparent reaction barriers (8.7 and 7.9 kcal/mol, respectively). Instead, the hydride shift from the C_2 carbon to the C_1 carbon in the isomerization process is rate-limiting and requires an apparent activation energy of 22.3 kcal/mol at 343 K. This finding is consistent with the experimentally observed kinetic isotope effect, and the apparent activation energy also agrees with the previously reported experimental value of 21.2 ± 0.7 kcal/mol (343−373 K). In the hydride shift step, the Sn atom acts as a Lewis acid, which activates the acyclic form of glucose by polarizing the carbonyl group. On the other hand, the oxygen atom in the first coordination sphere of the active site acts as a Brønsted base, stabilizing the hydroxyl group on the C_2 carbon (see Figure 3).

The effects of the heteroatoms on the activities are examined by substituting Sn with Ti, Zr, V, Nb, Si, and Ge, in which the Sn and Zr sites are shown to be most active (see Table 2). Using energy decomposition analysis, it is shown that the reasons for Sn and Zr to be active are very different. For the Sn site, the oxygen atom that acts as a Brønsted base in the rate-limiting step carries a high negative charge (Q_O), so that the transition state is greatly stabilized by strong electrostatic interactions. On the other hand, because Zr has the largest radius (R), it is the most polarizable metal atom of those examined, and therefore the Zr site has the lowest energy penalty associated with geometric distortion of the site from its resting geometry to the geometry in the transition state. Hence, two physical properties, metal atom polarizability and Brønsted basicity of the associated O atom, control the reaction barrier of the rate-limiting step in the isomerization of glucose to fructose in M-BEA. The more open partially hydrolyzed site is preferred relative to a closed site because its greater flexibility leads to a lower geometric distortion penalty.

■ ASSOCIATED CONTENT

Supporting Information

Additional information as noted in the text, including structural data, equilibrium and apparent activation energy calculations, and discussions of energy decomposition analysis. This information is available free of charge via the Internet at http://pubs.acs.org/.

■ AUTHOR INFORMATION

Corresponding Author

*E-mail: alexbell@berkeley.edu.

Notes

The authors declare no competing financial interest.

■ ACKNOWLEDGMENTS

This work was supported by the XC^2 program funded by BP.

■ REFERENCES

(1) Román-Leshkov, Y.; Barrett, C. J.; Liu, Z. Y.; Dumesic, J. A. *Nature* **2007**, *447*, 982−985.

(2) Rosatella, A. A.; Simeonov, S. P.; Frade, R. F. M.; Afonso, C. A. M. *Green Chem.* **2011**, *13*, 754.

(3) West, R. M.; Liu, Z. Y.; Peter, M.; Dumesic, J. A. *ChemSusChem* **2008**, *1*, 417−424.

(4) Huber, G. W.; Chheda, J. N.; Barrett, C. J.; Dumesic, J. A. *Science* **2005**, *308*, 1446−1450.

(5) Antal, M. J., Jr.; Mok, W. S. L.; Richards, G. N. *Carbohydr. Res.* **1990**, *199*, 91−109.

(6) Kuster, B. F. M. *Starch/Staerke* **1990**, *42*, 314−321.

(7) Zakrzewska, M. E.; Bogel-Łukasik, E.; Bogel-Łukasik, R. *Chem. Rev.* **2011**, *111*, 397−417.

(8) Binder, J. B.; Raines, R. T. *J. Am. Chem. Soc.* **2009**, *131*, 1979−1985.

(9) Zhao, H.; Holladay, J. E.; Brown, H.; Zhang, Z. C. *Science* **2007**, *316*, 1597−1600.

(10) Qi, X.; Watanabe, M.; Aida, T. M.; Smith, R. L., Jr. *Green Chem.* **2009**, *11*, 1327.

(11) Chan, J. Y. G.; Zhang, Y. *ChemSusChem* **2009**, *2*, 731−734.

(12) Lansalot-Matras, C.; Moreau, C. *Catal. Commun.* **2003**, *4*, 517−520.

(13) Hu, S.; Zhang, Z.; Song, J.; Zhou, Y.; Han, B. *Green Chem.* **2009**, *11*, 1746.

(14) Qi, X.; Watanabe, M.; Aida, T. M.; Smith, R. L. *ChemSusChem* **2010**, *3*, 1071−1077.

(15) Ilgen, F.; Ott, D.; Kralisch, D.; Reil, C.; Palmberger, A.; König, B. *Green Chem.* **2009**, *11*, 1948.

(16) Chidambaram, M.; Bell, A. T. *Green Chem.* **2010**, *12*, 1253.

(17) Gallezot, P. *Chem. Soc. Rev.* **2012**, *41*, 1538.

(18) Moliner, M.; Román-Leshkov, Y.; Davis, M. E. *Proc. Natl. Acad. Sci. U.S.A.* **2010**, *107*, 6164−6168.

(19) Nikolla, E.; Román-Leshkov, Y.; Moliner, M.; Davis, M. E. *ACS Catal* **2011**, *1*, 408−410.

(20) Bermejo-Deval, R.; Assary, R. S.; Nikolla, E.; Moliner, M.; Román-Leshkov, Y.; Hwang, S.-J.; Palsdottir, A.; Silverman, D.; Lobo, R. F.; Curtiss, L. A.; Davis, M. E. *Proc. Natl. Acad. Sci.* **2012**, *109*, 9727−9732.

(21) Román-Leshkov, Y.; Moliner, M.; Labinger, J. A.; Davis, M. E. *Angew. Chem., Int. Ed.* **2010**, *49*, 8954−8957.

(22) Boronat, M.; Concepción, P.; Corma, A.; Renz, M.; Valencia, S. *J. Catal.* **2005**, *234*, 111−118.

(23) Boronat, M.; Corma, A.; Renz, M. *J. Phys. Chem. B* **2006**, *110*, 21168−21174.

(24) Bermejo-Deval, R.; Gounder, R.; Davis, M. E. *Acs Catal.* **2012**, *2*, 2705−2713.

(25) Gomes, J.; Zimmerman, P. M.; Head-Gordon, M.; Bell, A. T. *J. Phys. Chem. C* **2012**, *116*, 15406−15414.

(26) Yang, G.; Pidko, E. A.; Hensen, E. J. M. *ChemSusChem* **2013**, *6*, 1688−1696.

(27) Rai, N.; Caratzoulas, S.; Vlachos, D. G. *ACS Catal.* **2013**, *3*, 2294−2298.

(28) Khaliullin, R. Z.; Cobar, E. A.; Lochan, R. C.; Bell, A. T.; Head-Gordon, M. *J. Phys. Chem. A* **2007**, *111*, 8753−8765.

(29) Newsam, J. M.; Treacy, M. M. J.; Koetsier, W. T.; Gruyter, C. B. D. *Proc. R. Soc. Lond. Ser. Math. Phys. Sci.* **1988**, *420*, 375−405.

(30) Bare, S. R.; Kelly, S. D.; Sinkler, W.; Low, J. J.; Modica, F. S.; Valencia, S.; Corma, A.; Nemeth, L. T. *J. Am. Chem. Soc.* **2005**, *127*, 12924−12932.

(31) Shetty, S.; Pal, S.; Kanhere, D.; Goursot, A. *Chem. - Eur. J.* **2005**, *12*, 518−523.

(32) Zimmerman, P. M.; Head-Gordon, M.; Bell, A. T. *J. Chem. Theory Comput.* **2011**, *7*, 1695−1703.

(33) Foloppe, N.; MacKerell, A. D., Jr. *J. Comput. Chem.* **2000**, *21*, 86−104.

(34) Yin, D.; MacKerell, A. D. *J. Comput. Chem.* **1998**, *19*, 334−348.

(35) Vanommeslaeghe, K.; Hatcher, E.; Acharya, C.; Kundu, S.; Zhong, S.; Shim, J.; Darian, E.; Guvench, O.; Lopes, P.; Vorobyov, I.; Mackerell, A. D. *J. Comput. Chem.* **2010**, *31*, 671−690.

(36) Li, Y.-P.; Gomes, J.; Sharada, S. M.; Bell, A. T.; Head-Gordon, M. University of California, Berkeley, CA. Unpublished work, 2013.

(37) Zoete, V.; Cuendet, M. A.; Grosdidier, A.; Michielin, O. *J. Comput. Chem.* **2011**, *32*, 2359−2368.

(38) Chai, J.-D.; Head-Gordon, M. *Phys. Chem. Chem. Phys.* **2008**, *10*, 6615−6620.
(39) Chai, J.-D.; Head-Gordon, M. *J. Chem. Phys.* **2008**, *128*, 084106−084115.
(40) Shao, Y.; Molnar, L. F.; Jung, Y.; Kussmann, J.; Ochsenfeld, C.; Brown, S. T.; Gilbert, A. T. B.; Slipchenko, L. V.; Levchenko, S. V.; O'Neill, D. P.; DiStasio, R. A., Jr; Lochan, R. C.; Wang, T.; Beran, G. J. O.; Besley, N. A.; Herbert, J. M.; Lin, C. Y.; Voorhis, T. V.; Chien, S. H.; Sodt, A.; Steele, R. P.; Rassolov, V. A.; Maslen, P. E.; Korambath, P. P.; Adamson, R. D.; Austin, B.; Baker, J.; Byrd, E. F. C.; Dachsel, H.; Doerksen, R. J.; Dreuw, A.; Dunietz, B. D.; Dutoi, A. D.; Furlani, T. R.; Gwaltney, S. R.; Heyden, A.; Hirata, S.; Hsu, C.-P.; Kedziora, G.; Khalliulin, R. Z.; Klunzinger, P.; Lee, A. M.; Lee, M. S.; Liang, W.; Lotan, I.; Nair, N.; Peters, B.; Proynov, E. I.; Pieniazek, P. A.; Rhee, Y. M.; Ritchie, J.; Rosta, E.; Sherrill, C. D.; Simmonett, A. C.; Subotnik, J. E.; Iii, H. L. W.; Zhang, W.; Bell, A. T.; Chakraborty, A. K.; Chipman, D. M.; Keil, F. J.; Warshel, A.; Hehre, W. J.; Iii, H. F. S.; Kong, J.; Krylov, A. I.; Gill, P. M. W.; Head-Gordon, M. *Phys. Chem. Chem. Phys.* **2006**, *8*, 3172−3191.
(41) Foster, J. P.; Weinhold, F. *J. Am. Chem. Soc.* **1980**, *102*, 7211−7218.
(42) Behn, A.; Zimmerman, P. M.; Bell, A. T.; Head-Gordon, M. *J. Chem. Phys.* **2011**, *135*, 224108.
(43) Gounder, R.; Davis, M. E. *J. Catal.* **2013**, *308*, 176−188.
(44) Marenich, A. V.; Olson, R. M.; Kelly, C. P.; Cramer, C. J.; Truhlar, D. G. *J. Chem. Theory Comput.* **2007**, *3*, 2011−2033.
(45) Tielens, F.; Dzwigaj, S. *Chem. Phys. Lett.* **2010**, *501*, 59−63.
(46) Politzer, P.; Jin, P.; Murray, J. S. *J. Chem. Phys.* **2002**, *117*, 8197−8202.
(47) *CRC Handbook of Chemistry and Physics*, 93rd ed.; Haynes, W. M., Ed.; CRC Press: Boca Raton, FL, 2013.